Control Strategy for DAB using SPS for Integration of Modular Batteries in EV

Alberto Cárcamo[1], Aitor Vázquez[1], Alberto Rodríguez[1], Diego G. Lamar[1], Marta M. Hernando[1], Alexis A. Gómez[1], Daniel Remón[2]

[1]University of Oviedo, [2]E+ Ecoeficiencia e Ingeniería S.L.
[1]Gijón, Spain; [2]Gijón, Spain
[1]carcamoalberto@uniovi.es; [2]innovacion@emasingenieria.es
[1] https://sea.grupos.uniovi.es/; [2] https://www.emasingenieria.es/

KEYWORDS

«Dual Active Bridge (DAB) DC-DC converter», «DC-DC power converter», «Control strategy », «Battery charger», «Electric Vehicle (EV)».

ABSTRACT

This paper explores a control strategy for a Dual Active Bridge (DAB) used for the integration of removable batteries on Electric Vehicles (EVs). It uses Single Phase Shift (SPS) control at different switching frequencies to increase power and extend Zero Voltage Switching (ZVS), while it works in burst mode at low power.

INTRODUCTION

The global commitment on the reduction of CO_2 emissions through legislation, especially in the European Union [1], has encouraged the research and development on Electric Vehicles (EVs) in many countries around the world. Although most EVs have only one Energy Storage System (ESS), which is typically a non-removable battery, there have been some proposals for using removable batteries to allow battery swapping [2], [3].

This project is done with the industry with the goal of integrating removable batteries to EVs that already have a non-removable battery as the main ESS. The addition of removable batteries increases the flexibility of the energy management and may allow to extend the EV range.

The integration of additional batteries to an EV can be done through a bidirectional power converter such as the Dual Active Bridge (DAB), which is a well-known topology, that has been thoroughly studied and proven to be suitable when compared to others as it offers a high power density and high efficiency due to the operation under Zero Voltage Switching (ZVS) [4]–[8].

Fig. 1 shows a diagram of the EV power system, where the DAB converter interfaces the removable batteries to the high voltage (HV) dc-bus, connected in parallel with the non-removable battery.
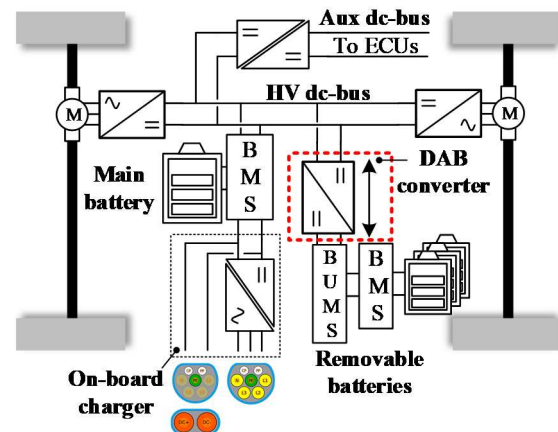

Fig. 1. EV power system diagram.

Fig. 2 shows the control scheme used in the integration of the removable battery and the

converter into the EV power system, where three main parts can be identified. The first one is the Battery Management System (BMS), which among other functions, measures all the internal parameters of the battery pack, such as cell voltage, temperature, current, etc. The second element is the Battery Unit Management System (BUMS), which is responsible for the energy management of the integrated system, and the third element is the DAB converter, which is responsible for the energy transfer between the removable batteries and the EV powertrain.

For implementing the control of the energy management of the integrated system, a cascade control loop is implemented, as shown in Fig. 2, where the BUMS executes a power controller as the outer control loop, providing the current reference, i_{ref}, for the current controller that is the inner control loop of the DAB. The BUMS communicates with the BMS and with the DAB via RS-485 and via Controller Area Network (CAN) protocols, respectively. It also communicates through an external Electronic Control Unit (ECU) with the power system of the EV.
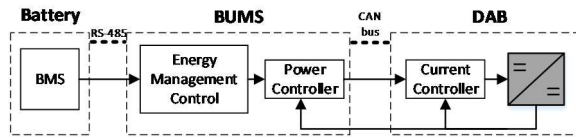

Fig. 2. Integration of the removable batteries and DAB diagram.

This paper focuses on the control strategy of the DAB, in which multiple operational modes are considered in function of the current reference provided by the BUMS (and, by extension, with the electrical powertrain and battery status). Therefore, a control strategy is investigated for different operation scenarios, along with their transitions and the impact on the converter performance.

CONTROL STRATEGY OF THE DAB

The control strategy of the DAB converter consists of the implementation of 2 different operation modes, which depends on the secondary side current reference, i_{ref}. The 2 operation modes are the following: closed loop and burst mode.

The following analysis is done assuming a positive power transfer, from the primary side to the secondary side, implying a positive phase shift. Although all the analysis is done assuming this condition, it is important to clarify that it is valid regardless of the direction of the power transfer.

The DAB converter schematic is shown in Fig. 3, where removable batteries are the primary side voltage, V_1, and V_2 is the HV dc-bus (provided by the non-removable battery). The leakage inductance, L_{Lk}, represents the sum of the transformer leakage inductance and an external inductor.
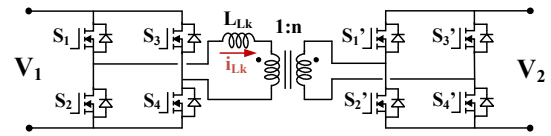

Fig. 3. DAB converter schematic.

There are several control methods for the DAB converter, such as Single Phase Shift (SPS), Double Phase Shift (DPS), Triple Phase Shift (TPS) [9]–[11]. For this project, the converter works exclusively in SPS, which consists of the branches working with a 50% duty cycle, while the phase shift between both full-bridges regulates the power transfer. SPS is a relatively simple control method, which demands low computational resources, allowing the DSP to perform other tasks such as communications of the control of additional converters.

This topology allows the converter to work with ZVS, although this operating condition is not always guaranteed, particularly for low power or wide voltage range. There are many ways in which ZVS can be guaranteed for all the power range, such as using the transformer magnetizing inductance [12], or working with other control methods [13], [14].

With SPS, the DAB converter is not able to operate with ZVS throughout all the power range, as it must have a minimum current for charging/discharging the parasitic capacitors of the MOSFETs. The ZVS condition also depends on the relationship between the voltages at both sides, which is defined as:

$$M = \frac{V_2}{n \cdot V_1} \qquad (1)$$

where n is the turns ratio of the transformer.

Fig. 4 shows the current through the inductor, i_{Lk}, with SPS operation, where i_1 and i_2, are the values of the current at the switching instant of the primary side and the secondary side, respectively, along the switching period, T. These currents must be positive in order to get ZVS, and big enough to discharge the parasitic capacitances.
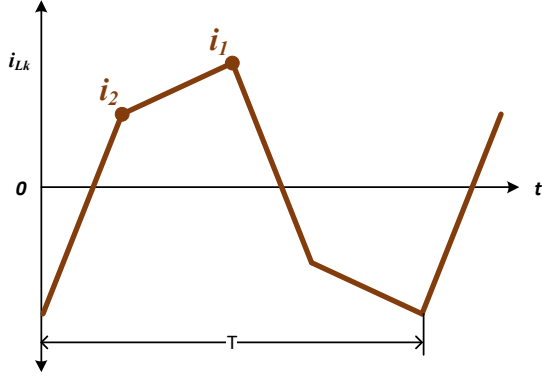

Fig. 4. DAB converter i_{Lk} waveform during a switching period, T, at the switching instant of the primary side, i_1, and the secondary side, i_2.

The value of the currents at i_1 and i_2 as a function of the phase shift, φ, the switching frequency, f_s, and the voltages, V_1 and V_2, is given by [12]:

$$i_1 = \frac{1}{4\pi f_s L_{Lk}} \left(V_1 \pi + \frac{V_2}{n} \frac{2k}{2k+1} \ (2\varphi - \pi) \right) \frac{2k+1}{2k+\frac{1}{2}} \quad (2)$$

$$i_2 = \frac{1}{4\pi f_s L_{Lk}} \left(V_1 (2\varphi - \pi) + \frac{V_2}{n} \frac{2k}{2k+1} \pi \right) \frac{2k+1}{2k+\frac{1}{2}} \quad (3)$$

where k is the ratio of the transformer magnetizing inductance, L_m, and the leakage inductance, L_{Lk}, given by [12]:

$$k = \frac{L_m}{L_{Lk}} \quad (4)$$

These equations are used to estimate the minimum phase shift where i_1 and i_2 are big enough to ensure ZVS at the primary side, at the worst possible scenario of M. The same process, with similar equations, is applied for ensuring ZVS at the secondary side.

The minimum power for ensuring ZVS is given by [12]:

$$P_{min} = \frac{V_1 V_2 \varphi_{min}(\pi - \varphi_{min})}{2\pi^2 n f_s L_{Lk}} \frac{2k}{2k + \frac{1}{2}} \quad (5)$$

where φ_{min} is the minimum phase shift needed for ZVS operation, which is obtained using previous equations.

Frequency Steps

As mentioned before, the DAB converter proposed in this paper operates using SPS. Although the maximum power is achieved at 90° phase shift, for this project, 63° is chosen as the maximum phase shift. This figure is selected for keeping the linearity between the power and the phase shift, as it can be seen from the power curves in Fig. 5 that above 63° the linearity begins to decrease.

The converter is designed to operate at a switching frequency of 75 kHz, which allows it to reach a maximum power of 4.4 kW with the selected value of L$_{Lk}$ (given in Table 2). However, it is possible to extend its maximum power by decreasing this switching frequency. Therefore, by defining a new switching frequency of 35 kHz, the maximum power is increased to 9.4 kW, approximately. Using two frequencies reduces the reactive current and allows the converter to work in a wider power range with ZVS.

By operating the converter with different frequencies, some aspects are considered for the points where a change in frequency occur, defined as a frequency step. At a frequency step, as the switching frequency changes, also does the sampling frequency. This is due to the sample time of the ADC being configured to work at switching frequency, which is known as synchronous sampling. Therefore, it is necessary to update the PI controller constants, to match the corresponding sampling frequency.

Another important aspect at a frequency step is the phase shift compensation. As the frequency is changing abruptly, the phase shift angle must be compensated with a feed-forward, to avoid any oscillations, as stepping from one frequency to another without a phase shift compensation, would make the power increase or decrease instantaneously, affecting the controller in a negative way. The phase shift compensations, as well as the PI controller constants are predefined values at each frequency step point.

Fig. 5 shows the converter control path (black), with the frequency step points marked with letters B-E and the burst Mode, used to extend ZVS at low power, marked with letters G-F.

The figure shows the power curves of the converter in function of the phase shift angle, for switching frequencies of 35 kHz (blue) and 75 kHz (red). There is also a green area which describes the burst Mode region. The control path is the path over the power curves that the converter follows, depending on the i_{ref}, with a hysteresis added to avoid oscillations among frequency steps and also when entering or exiting the burst Mode. The blue and red dashed lines, show the minimum power for ZVS operation for 35 and 75 kHz, respectively. The maximum power is marked with the letter A and a vertical black dashed line, at 63°.
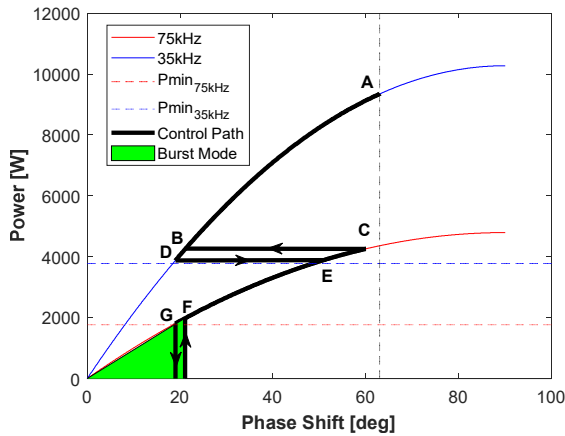

Fig. 5. Control path (black) over the power curves at switching frequencies of 35 (blue) and 75 kHz (red), and the burst mode area (green). The letters show where the frequency steps occur (B-E) and transition to and from burst mode (G, F).

For this project, the converter is not expected to work most of the time neither at maximum power nor at low power, but rather between points F and E, from Fig. 5. The optimal points where a frequency step occurs, are determined by the minimum power needed for ZVS operation, using (5), which is 3.76 and 1.75 kW for 35 and 75 kHz, respectively.

Burst Mode

The converter operates in burst mode in the low power region shown in green in Fig. 5, to extend the ZVS range, as the converter is no longer able to work with ZVS using SPS [7]. The burst mode consists of turning on/off the converter, at a fixed phase shift, φ_B, during a percentage of time from a defined period. In this application, the burst mode is configured to operate at 300 Hz, with the percentage of time of the converter on, defined as the burst duty cycle, d_B.

$$d_B = \frac{i_{ref}}{i_B} \qquad (6)$$

where i_B is the current at φ_B.

For this specific application, the converter is only expected to work in this mode in exceptional cases, as it is not mandatory for the removable battery to work at low power, although it will depend on the energy management control configuration, which is out of the scope of this paper.

Fig. 6 shows a block diagram for the control strategy, where the control algorithm feeds the PWM with the switching frequency and controls the switch that selects the operation mode, either closed loop control or burst mode operation. The operation mode is selected in function of the value of i_{ref}, and the output of
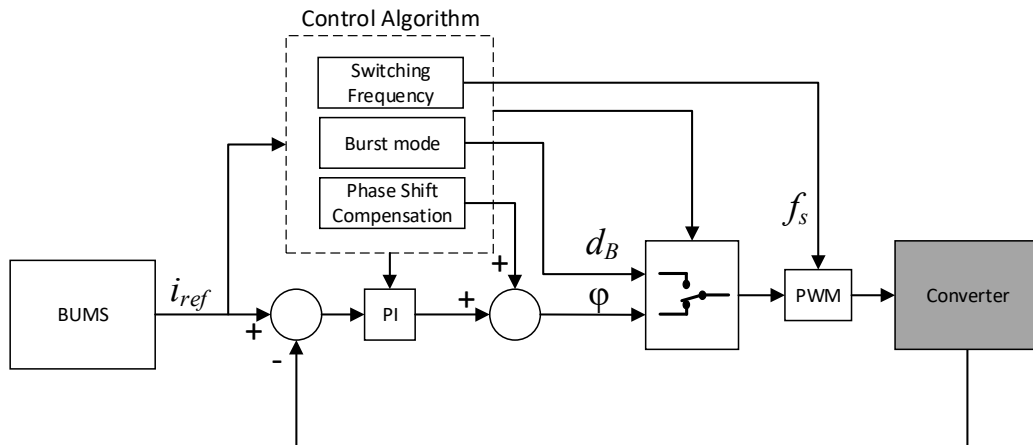

Fig. 6. Control strategy block diagram.

the switch is either the phase shift, for closed loop control, or the d_B, for burst mode. It also shows the phase shift compensation as a feed forward, where it is important to mention that this happens only once during a frequency step and that it is a constant predefined value. As described in the first section, the BUMS is an external device, which is responsible for the energy management, among other things, and is the one that executes the power loop and sends the current reference i_{ref} to the converter DSP.

DAB Converter Prototype

Fig. 7 shows the DAB prototype built in the lab for the validation of the control strategy. Several subsystems can be distinguished: the power stage, the control stage, drivers, and sensors. Table 1 shows some of the components used.

Table 1: Main Components List

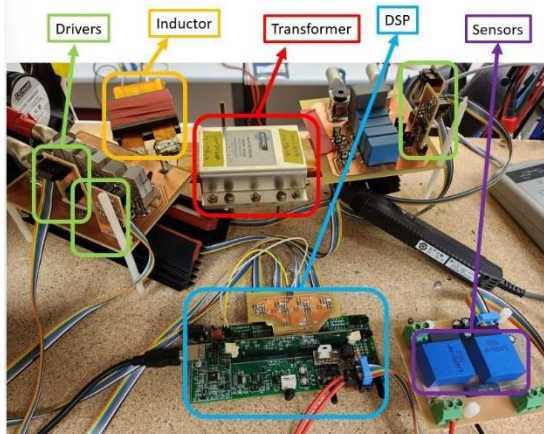| Primary side MOSFETs	IXTQ180
Secondary side MOSFETs	IPWS65R075CFD7A
Voltage sensor	LV 25-P
Current sensor	LA 25-NP
Drivers	Si8233
DSP	TI F28335
Inductor core material	3F3

Fig. 7. DAB converter prototype.

An important element of the DAB converter is the inductor. For this prototype, the inductor is made up of a planar core, with one turn, placed on the primary side of the converter. This design has proven through experimentation to be the most efficient compared to other designs with E-cores, which are not shown in this paper. Also, in [15] it is shown that it presents the best results when compared with other planar designs.

EXPERIMENTAL RESULTS

Table 2 shows the DAB parameters and conditions under which the preliminary experimental results are obtained. The experimental setup consists in using two commercial Power Supplies, one at the primary side instead of a battery due to safety concerns, and the other one at the secondary side to simulate the HV dc-bus.

Table 2 DAB Converter Parameters

V_1 [V]	54-66
V_2 [V]	390-470
$L_{Lk} = L + L_k$ [µH]	1.182
n	7
f_s [kHz]	35 and 75
L_k [nH]	142
L_m [µH]	24
L [µH]	1.04

The waveform for i_{Lk} in closed loop at a frequency step from 35 to 75 kHz is shown in Fig. 8, where it can be seen that the transition happens almost instantaneously and takes approximately 5 to 6 switching periods to settle. The converter manages the same power with both frequencies without any visible dynamics due to the phase shift compensation, which allows the frequency jump to happen smoothly without affecting the current controller.

Fig. 9 shows the waveforms of the converter working at 7 kW in steady state, where (a) shows V_{GS} of MOSFETs S2' and S4', and V_{DS} for the latter, and (b) shows the current i_{Lk}.

The current i_{Lk} working in burst mode operation is shown in Fig. 10, with a d_B of 50% and a frequency of 303 Hz. Other tests were performed at frequencies of the range of 3 kHz, with similar results, although they are not shown in this paper. The drawback of this operation mode is that these frequencies are in the audible range, however it is not relevant, as the converter is expected to work on this mode just in exceptional cases.
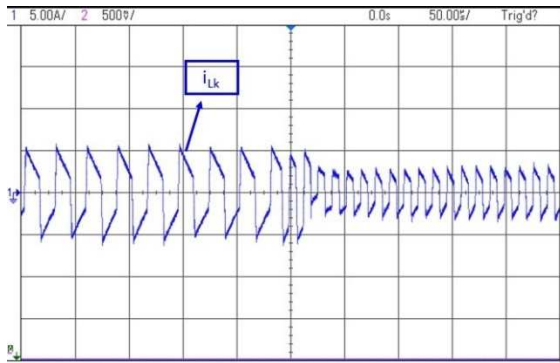
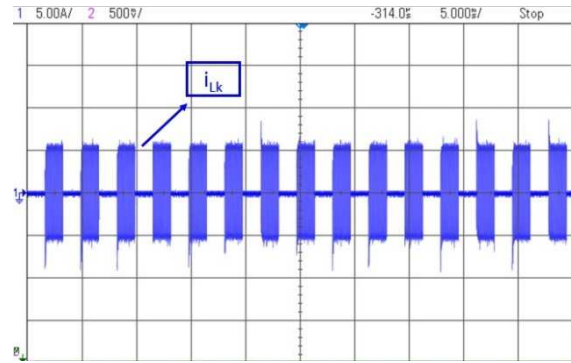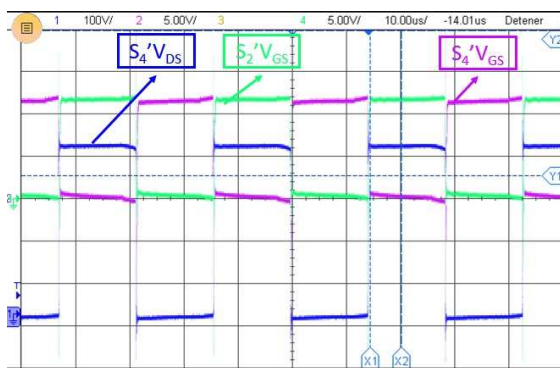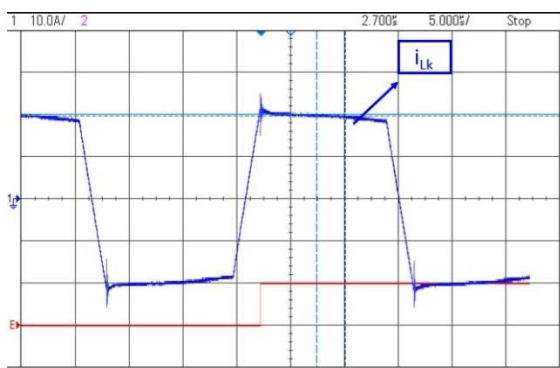Fig. 8. Current, i_{Lk} waveform at a frequency step from 35 kHz to 75 kHz.

Fig. 10. DAB converter working in burst mode with $d_B = 50\%$ and a frequency of 303 Hz.

The efficiency of the converter is evaluated at both switching frequencies, where Fig. 11 shows it as a function of the phase shift, while Fig. 12 shows the efficiency as a function of the power. In Fig. 11, it can be appreciated that the efficiency for both frequencies is very similar at low phase shift, this is because the reactive current increases with the phase shift, reducing the efficiency. At 35 kHz, the efficiency tends to be lower; this is mainly due to conduction losses, as the power, and thus the current is more than double when switching at 35 kHz, than when switching at 75 kHz with the same phase shift.

(a)

(b)

Fig. 9. DAB converter waveforms working at 7 kW. (a) V_{DS} and V_{GS} are shown for switch S_4' and switches S_2' and S_4', respectively. (b) Current i_{Lk} is shown.
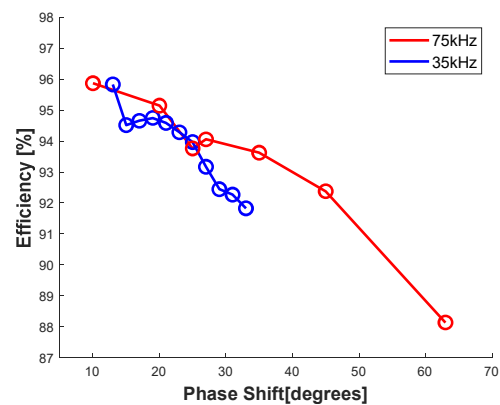

Fig. 11. DAB converter efficiency in function of the phase shift for 35 (blue) and 75 kHz (red).

Fig. 12 shows approximately where the frequency step occurs (black dashed line), where one clear advantage of working with another switching frequency can be appreciated, as it allows to increase the power at a lower phase shift, therefore operating with

a lower reactive current, thus increasing the efficiency of the converter. It is evident that the frequency jump happens when the efficiency is under 90%, implying that using more than 2 frequencies should be considered for reducing the reactive currents and to maintain a high efficiency operation.
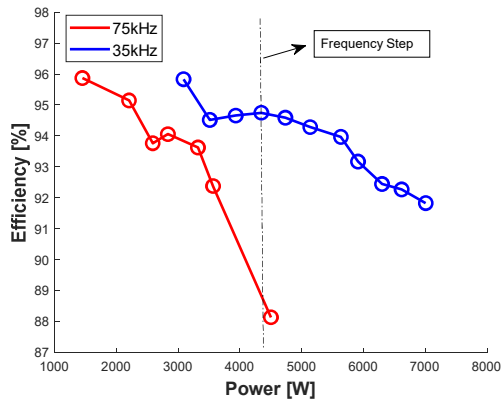

Fig. 12. DAB converter efficiency in function of the power for 35 (blue) and 75 kHz(red) switching frequencies.

CONCLUSIONS AND FUTURE WORK

The DAB converter prototype working with SPS is analyzed for the integration of removable batteries in an EV system, where a control strategy involving the use of 2 switching frequencies and a burst mode is evaluated through experimentation to assess their impact on the converter performance.

The results show that changing the switching frequency, to deal with the loss of ZVS at low power, has proven to have no impact on the closed loop control of the converter, while having more than one switching frequency also allows the converter to increase power with lower reactive currents and hence higher efficiency.

The burst mode is a good alternative for maintaining ZVS at low power, as it allows the converter to work on a predefined operation point, chosen at a high efficiency.

Moreover, a global strategy is developed to control the full system, using RS-485 and CAN communication protocols to send the proper variables to the high-level management systems of the batteries.

For future work, it is important to compare the proposed control strategy with others, such as DPS and TPS, to evaluate the performance and the trade-offs. The control strategy should consider introducing more switching frequencies in order to work with low reactive currents.

REFERENCES

[1]   European Commission, "Paris Agreement | Climate Action." https://ec.europa.eu/clima/policies/internati onal/negotiations/paris_en (accessed Jan. 17, 2022).

[2]   M. A. H. Rafi, R. Rennie, J. Larsen, and J. Bauman, "Investigation of fast charging and battery swapping options for electric haul trucks in underground mines," in *2020 IEEE Transportation Electrification Conference and Expo, ITEC 2020*, Institute of Electrical and Electronics Engineers Inc., Jun. 2020, pp. 1081–1087. doi: 10.1109/ITEC48692.2020.9161654.

[3]   Z. Chen, "The combination of battery swapping system and connected vehicles technology in intelligent transportation," *Proceedings - 2020 International Conference on Intelligent Transportation, Big Data and Smart City, ICITBS 2020*, pp. 72–75, 2020, doi: 10.1109/ICITBS49701.2020.00023.

[4]   F. Krismer, "Modeling and Optimization of Bidirectional Dual Active Bridge DC – DC Converter Topologies," ETH ZURICH, 2010.

[5]   M. Ryu, D. Jung, J. Baek, and H. Kim, "An optimized design of bi-directional dual active bridge converter for low voltage battery charger," in *16th International Power Electronics and Motion Control Conference and Exposition, PEMC 2014*, Institute of Electrical and Electronics Engineers Inc., Dec. 2014, pp. 177–183. doi: 10.1109/EPEPEMC.2014.6980709.

[6]   D. J. Costinett, "Analysis and Design of High Efficiency , High Conversion Ratio , DC-DC Power Converters," University of Colorado Boulder, 2013.

[7]   A. Rodríguez, A. Vázquez, D. G. Lamar, M. M. Hernando, and J. Sebastián, "Different purpose design strategies and techniques to improve the performance of a dual active bridge with phase-shift control," *IEEE Trans Power Electron*, vol. 30, no. 2, pp. 790–804, 2015, doi: 10.1109/TPEL.2014.2309853.

[8]   F. Krismer and J. W. Kolar, "Accurate small-signal model for the digital control of an automotive bidirectional dual active bridge," *IEEE Trans Power Electron*, vol. 24, no. 12, pp. 2756–2768, 2009, doi: 10.1109/TPEL.2009.2027904.

[9]   B. Zhao, Q. Song, and W. Liu, "Power characterization of isolated bidirectional dual-active-bridge dc-dc converter with dual-phase-shift control," *IEEE Trans Power Electron*, vol. 27, no. 9, pp. 4172–4176, 2012, doi: 10.1109/TPEL.2012.2189586.

[10]   H. Bai and C. Mi, "Eliminate reactive power and increase system efficiency of isolated bidirectional dual-active-bridge dc-dc converters using novel dual-phase-shift control," *IEEE Trans Power Electron*, vol. 23, no. 6, pp. 2905–2914, 2008, doi: 10.1109/TPEL.2008.2005103.

[11]   H. Gu, D. Jiang, R. Yin, S. Huang, Y. Liang, and Y. Wang, "Power characteristics analysis of bidirectional full-bridge DC-DC converter with triple-phase-shift control," *Proceedings of the 2015 10th IEEE Conference on Industrial Electronics and Applications, ICIEA 2015*, pp. 363–368, 2015, doi: 10.1109/ICIEA.2015.7334140.

[12]   K. Martín Diaz, "Análisis , diseño y construcción de un proveedor de bus para sistemas de distribución en corriente continua domésticos," Universidad de Oviedo, 2018.

[13]   F. Krismer and J. W. Kolar, "Closed form solution for minimum conduction loss modulation of DAB converters," *IEEE Trans Power Electron*, vol. 27, no. 1, pp. 174–188, 2012, doi: 10.1109/TPEL.2011.2157976.

[14]   C. Calderón, A. Barrado, A. Rodriguez, A. Lazaro, C. Fernández, and P. Zumel, "Dual active bridge with triple phase shift by obtaining soft switching in all operating range," in *2017 IEEE Energy Conversion Congress and Exposition (ECCE)*, 2017. doi: 10.1109/ECCE.2017.8096004.

[15]   Z. Zhang and M. A. E. Andersen, "High frequency AC inductor analysis and design for dual active bridge (DAB) converters," in *Conference Proceedings - IEEE Applied Power Electronics Conference and Exposition - APEC*, Institute of Electrical and Electronics Engineers Inc., May 2016, pp. 1090–1095. doi: 10.1109/APEC.2016.7468006.